Suppression of fast-ion-driven MHD instabilities by ECH/ECCD on Heliotron J

S. Yamamoto[1], K. Nagasaki[1], S. Kobayashi[1], K. Nagaoka[2], A. Cappa[3], H. Okada[1], T. Minami[1], S. Kado[1], S. Ohshima[1], S. Konoshima[1], Y. Nakamura[4], A. Ishizawa[4], G.M. Weir[5], N. Kenmochi[2], Y. Ohtani[4], X. Lu[4], Y. Tawada[4], D. Kokubu[4] and T. Mizuuchi[1]

[1] Institute of Advanced Energy, Kyoto University, Gokasho, Uji, Kyoto 611-0011, Japan
[2] National Institute for Fusion Science, Oroshi-cho 322-6, Toki, Gihu 509-5293, Japan
[3] Laboratorio Nacional de Fusión-CIEMAT, Av. Complutense 40. 28040, Madrid, Spain
[4] Graduate School of Energy Science, Kyoto University, Gokasho, Uji, Kyoto 611-0011, Japan
[5] Max-Planck-Institut für Plasmaphysik, EURATOM Association, Teilinstitut Greifswald, Germany

E-mail: yamamoto.satoshi.6n@kyoto-u.ac.jp

Abstract

Experiments of suppressing fast-ion-driven MHD instabilities such as energetic particle modes (EPMs) and global Alfvén eigenmodes (GAEs) have been made by using a second harmonic X-mode electron cyclotron heating (ECH) and current drive (ECCD) in the helical-axis heliotron device, Heliotron J. ECCD experiments show that the GAE destabilized by fast ions of neutral beam injection (NBI) with the observed frequency around 140 kHz are fully stabilized, and the EPMs with the observed frequency around 90 kHz are suppressed when the EC-driven plasma current flowing in the counter direction reaches approximately 0.7 kA. The low magnetic shear under the vacuum condition is modified into positive magnetic shear when counter-ECCD is applied, and the amplitude of GAEs and EPMs decreases with an increase of the EC-driven plasma current. These results indicate that magnetic shear is a key role in controlling GAEs as well as EPMs. The comparison of the calculation of shear Alfvén spectra with experimental results shows that the increasing continuum damping rate with an increase in local magnetic shear by EC-driven current is important for both EPMs and GAEs. Moreover, the increase in plasma current lead to the inward movement of GAEs. This effect would also contribute to suppression of GAEs because the continuum damping rate increases more and more toward core. Steady ECH is also found experimentally to be effective to control the amplitude of both GAEs and EPMs. The amplitude of EPMs, and especially for GAEs decreases with an increase in the ECH power under fixed density conditions.

1. Introduction

Good confinement of fast particles such as alpha particles is needed to sustain a self-ignited plasma, and/or to heat and control plasmas in a fusion reactor. Fast particles whose velocity are near the Alfvén velocity can

resonate with magnetohydrodynamics (MHD) waves, and excite MHD waves with weak damping by the energy transfer from fast particles to MHD waves due to a resonant wave-particle interaction. Unstable MHD waves enhance anomalous transport of fast particles, and then these will induce flattening of fast particle profile resulting in the decrease in fusion gain Q [1-4]. They also induce a loss of fast particles causing damage of first wall components. On the other hand, MHD waves can be applied to an MHD spectroscopy [5, 6] to measure the safety factor profile and deuterium-tritium ratio, and direct ion heating by fast particles via alpha channeling [7]. We have to clarify a physical mechanism of the resonant wave-particle interaction in the fusion reactor. Moreover, we also have to develop a method to control and/or suppress the fast-particle-driven MHD instabilities such as Alfvén eigenmodes (AEs) and energetic particle modes (EPMs). If a technical scheme of suppressing a particular type of AEs can be developed, it would be advantageous for prevention of excessive fast particle losses and damage of first wall components. It would also provide the opportunity to investigate properties of specific fast-ion-driven MHD instabilities.

Electron cyclotron heating (ECH) and current drive (ECCD) are a useful tool for stabilizing MHD instabilities such as neoclassical tearing mode (NTM) in a tokamak [8, 9]. It is an ideal tool for controlling MHD instabilities since it can provide highly localized power deposition and toroidal current with a known location and good controllability, which significantly changes electron temperature and/or rotational transform (safety factor). Stabilization/Destabilization of AEs by ECH has been reported on the DIII-D tokamak for the first time [10-12]. In high beta plasmas of the DIII-D tokamak, reversed shear AEs (RSAEs) were stabilized with localized ECH which was deposited at off-axis minimum in safety factor $q_{\min}$. These observations can be explained by that the RSAE minimum frequency increases and overcomes the TAE frequency due to an increase in local electron temperature and its gradient by ECH [12]. Effect of ECH on AEs was also experimentally studied in the TJ-II stellarator/heliotron (S/H) device [13]. Some continuous AEs were changed into chirping ones in association with the decrease in their amplitude when ECH was additionally applied to NBI-heated plasmas. Effects of the magnetic configuration such as rotational transform and magnetic well on the AEs was also reported in TJ-II [14, 15].

EPMs were successfully stabilized by ECCD in the S/H device, Heliotron J [16, 17]. The low magnetic shear configuration is changed into the middle magnetic shear configuration by the EC-driven plasma current, and low m/n (m and n are the poloidal and toroidal mode number) EPMs excited at the edge region are fully stabilized when the magnetic shear reaches a threshold value. Both co- and counter-ECCD suppress the EPMs, indicating that magnetic shear is effective regardless of its sign. Here co-direction is defined as the direction

for the driven current to increase the rotational transform. The cause of EPM suppression was speculated by the increasing continuum damping rate which is related to the absolute value of magnetic shear [18, 19]. It is natural to assume that the main damping mechanism of the EPM is continuum damping because the EPM is the shear Alfvén continuum forcedly destabilized by the fast ion contribution. One of the purposes of this article is to study the stabilization of not only EPMs but also global AEs (GAEs) by ECCD in Heliotron J. We also qualitatively assess the mechanism of ECCD effects on both EPMs and GAEs due to the change of shear Alfvén spectra resulting from the increase in EC-driven plasma current. In addition to ECCD effects, we show suppression of both EPMs and GAEs by ECH in Heliotron J. This suppression cannot be explained by the same physical mechanism of the DIII-D plasma because experimental conditions and the magnetic configuration of Heliotron J are different from those of DIII-D. On the other hand, the characteristics of the RSAE observed in reversed shear tokamaks are similar to GAE because they are not frequency gap modes and localize the low magnetic shear region. Understanding of GAEs suppression may be helpful to suppress RSAEs in tokamaks.

This article is organized as follows. The experimental setup of the Heliotron J device in this work is introduced in Sec. 2. Section 3 presents effects of ECCD and ECH on both EPMs and GAEs. Comparison of experimental observations, including the observed frequencies and mode profiles, with calculated shear Alfvén spectra for the qualitative estimation of the ECCD effect on EPMs and GAEs is discussed in Sec. 4. Section 5 summarizes the main results of this work and concludes the paper.

2. Experimental Setup

The Heliotron J device is a medium-sized helical-axis heliotron device whose major and minor radii are $R = 1.2$ m and $\langle a \rangle < 0.25$ m, respectively [20, 21]. Heliotron J aims to obtain simultaneously both high MHD stability and good particle confinement by partially optimized quasi-omnigenous magnetic configuration with low magnetic shear based on the helical-axis heliotron concept. The magnetic configuration of the Heliotron J plasma is mainly composed of toroidicity, helicity and bumpiness. Bumpiness is the toroidal Fourier harmonic of a magnetic field. Trapped particles are expected to be confined ideally in a well of magnetic field strength "bumpiness" where the drift surface of the trapped particle is close to a magnetic flux surface. The magnetic configuration of Heliotron J basically has low magnetic shear s ($s = a/\iota \cdot \mathrm{d}\iota/\mathrm{d}r < 0.02$ in a vacuum, here $\iota/2\pi$ and r being the rotational transform and minor radius, respectively) in order to avoid crossing rational surfaces with a low mode number and magnetic well to have good MHD stability with respect to pressure-driven MHD instabilities in the whole plasma region. The poloidal magnetic field is so weak and the magnetic shear is so

low that small external current of a few kA can easily modify the rotational transform profile compared to tokamaks and high magnetic shear S/H device such as LHD. This feature lead that Heliotron J is advantageous to study the effect of ECH/ECCD on fast-ion-driven MHD instabilities.

In previous experiments which were operated in the magnetic configuration with the rotational transform $\iota/2\pi$~0.51, and weak magnetic well or magnetic hill at the edge, we observed both pressure-driven MHD instabilities and fast-ion-driven EPMs. We chose the magnetic configuration with the rotational transform $\iota/2\pi$~0.56 and magnetic well in a whole plasma region in order to avoid pressure-driven MHD instabilities, e.g. m=2/n=1 mode, and in order to have GAEs, which is usually observed in S/H plasmas with low magnetic shear in Heliotron J [22], TJ-II and W7-AS [23].

Regarding fast-particle-driven MHD instabilities, there is no frequency gap for toroidicity-induced AE (TAE) with a low mode number, e.g. n=1, 2, 3.. in the most cases of the Heliotron J plasma because low-n shear Alfvén continua do not intersect with each other due to low magnetic shear. However, GAE, which can lie just above and/or below each shear Alfvén continuum, can be destabilized by fast particles instead of low-n TAE.

Plasma experiments in Heliotron J are basically carried out around magnetic field strength at magnetic axis, B_0 = 1.25 T, to produce the plasma by a 2nd harmonics X-mode 70GHz ECH [24]. Additional heating can be provided by co and counter tangential neutral beam injections (NBIs) of hydrogen at the injection energy of E < 27 keV and each injection power of P < 700 kW. Working gas is deuterium in our experiments. Maximum injection ECH power is about P_{ECH} = 350 kW and the focused EC beam radius at $1/e^2$ power of 0.03 m makes the power deposition and driven current localized in the radial direction, which is much smaller than the averaged minor plasma radius. The heating position and profile of ECH can be varied by the changing of ECH injection angles in the poloidal direction and/or the changing of magnetic field strength in Heliotron J. The magnitude and direction of EC-driven plasma current can be controlled by the angle of the ECH launcher mirror to control the refractive index of EC waves along a magnetic field line $N_{||}$, and the direction of the magnetic field, respectively. Figure 1 (a) shows the radial profile of EC-driven plasma current density j_{EC} calculated by ray tracing code TRAVIS [25] under experimental conditions. The $N_{||}$ scan of ECCD indicates that TRAVIS predictions are consistent with measured plasma current by Rogowski coil within a factor of 2 in Heliotron J plasmas [16, 26].

Localized EC-driven current density at the plasma core derives strong changes in the rotational transform and induces magnetic shear in the whole plasma region as shown in Fig. 1 (b). The profile of the rotational transform is estimated by a simple model making addition of the poloidal magnetic field produced by EC-driven plasma current estimated by TRAVIS to the vacuum magnetic field of Heliotron J. It is difficult to include the fully localized plasma current near the plasma core as shown in Fig. 1 (a) into three-dimensional MHD equilibrium reconstruction by VMEC [27] because of representation format of plasma current in VMEC. Calculated rotational transform using the method as discussed above is consistent with VMEC result except for plasma core ($r/a < 0.5$), and we estimate magnetic shear based of the simple model. We discuss the effect of plasma current localized at plasma core on a shear Alfvén spectrum for the purpose of qualitative investigation of the effect of plasma current on EPMs and AEs in Sec. 4. Figure 1 (c) shows the profile of ECH deposition in ECH with P_{ECH}=240 kW and $N_{||}$=0.0 for Sec. 3.2. The profile of ECH and ECCD deposition is difficult to scan radially because ECH is the main heating source of plasma production in the Heliotron J device.

3. Effect of ECCD and ECH on AEs

Coherent electromagnetic fluctuations having frequency of $f_{obs} > 50$ kHz are usually observed in NBI-heated plasmas of Heliotron J. EPMs can be distinguished from AEs by the density dependence of the observed frequency of modes. Since the EPM is not a normal mode but a kinetic mode, frequency of EPMs is not proportional to Alfvén velocity having ion density dependence $\sim (n_i)^{-1/2}$, where n_i is ion density, but determined by the characteristic frequency of fast ions. Frequency of the EPM destabilized by passing ions, which are supplied by the tangential NBI, can be expressed as $(k_{//} \pm \iota/(2\pi R))v_{b//}$. Here $k_{//}$ being the parallel wave number can be expressed as $(n - 2\pi m/\iota)/R$, $v_{b//}$ the parallel velocity of the fast ion. In our experiment, calculated frequencies of EPMs destabilized by passing ions with injection energy of NBIs are approximately 1.5 times higher than the observed frequency of EPMs. This may be because the injection angle of the neutral beam (NB) is not parallel to the magnetic field even in the plasma core because of the helical-axis S/H plasma. If we consider the parallel velocity of fast ions, which destabilize the EPMs, calculated frequencies of EPMs seems to approach to observed EPMs frequencies. The Doppler shift of the mode frequency is negligible because toroidal rotation velocity is less than a few kHz in the experiment. The observed fluctuations having density dependence can be finally identified by comparison with shear Alfvén spectra calculated by STELLGAP and AE3D [28, 29] codes as GAEs, as will be discussed in Sec. 4.

3.1 *Effect of ECCD on AEs*

The experiments are carried out in the configuration with low bumpiness and under the low diamagnetic beta $<\beta_{dia}> \leqq 0.2$ %. $N_{\|}$ is scanned from -0.03 to 0.2 for the experiment to control EC-driven plasma current, and the ECH power is fixed as $P_{ECH} = 232$ kW in order to distinguish between ECH and ECCD effects. The electron density is linearly ramped up to 0.8×10^{19} m^{-3} in each $N_{\|}$ condition. Ramping up of the electron density in the discharge enables us to identify the observed modes as the EPM or GAE. Figure 2 shows the time evolution of power spectrum density (PSD) of the magnetic fluctuation db_θ/dt measured with the magnetic probe locating on the vacuum vessel in the case of (a) non-ECCD ($N_{\|} = 0.00$) and (b) ECCD ($N_{\|} = 0.15$), diamagnetic plasma stored energy, the line averaged electron density measured with a FIR interferometer, plasma current and the H_α signal. Here, b_θ being the poloidal component of the magnetic fluctuation. The solid line in blue and broken line in red correspond to the case of non-ECCD and ECCD experiments in Figs. 2 (c) ~ (f), respectively. We can see that main difference of plasma parameters are only plasma current and the magnetic fluctuation. After two NBIs are turned on, coherent magnetic fluctuations having frequency of $f_{obs} \sim 90$ kHz are observed in both $N_{\|}$ cases, and behavior of the observed modes is made clearly difference after $t = 0.21$ s. After this timing $t = 0.21$ s, the difference in plasma current between non-ECCD case and ECCD case is clearly seen in Fig. 2 (e). The amplitude of the observed modes in ECCD case (Fig. 2 (b)) is clearly smaller than that in non-ECCD case (Fig. 2 (a)) in all frequency ranges. These modes having the observed frequency of $f_{obs} \sim 90$ kHz are thought to be EPMs because of the weak density dependence. In Fig. 2 (a), the modes with the observed frequency $f_{obs} \sim 140$ kHz at $t = 0.28$ s is identified as GAE as will be discussed in Sec. 4 by the comparison with shear Alfvén spectra. GAEs are invisible in the case of ECCD as shown in Fig. 2 (b). The EPMs and GAE have mode number $m \sim 2/n = 1$ and $m \sim 4/n = 2$, respectively. Since poloidal mode number of observed modes estimated by phase differences of magnetic probes is sometimes indistinguishable between m and $m \pm 1$, we use not equal but tilde for representing poloidal mode number. We target on these EPMs and GAE to suppress and analyze in this article. We also observed other modes whose frequencies are higher than that of EPMs and GAE mentioned above and they have small amplitude and seems to be the higher harmonics of fundamental EPMs and GAE having $f_{obs} \sim 90$ kHz and 140 kHz. Mode amplitude b_θ/B_t of the observed EPMs and GAE is in the order of 10^{-6} at the magnetic probe position and they rotate in the diamagnetic drift direction of ions.

The stored energy measured with a diamagnetic loop is constant when $N_{\|}$ is scanned from 0.0 to 0.2 as shown in Fig. 2 (c). Thomson scattering, electron cyclotron emission (ECE) and charge exchange recombination spectroscopy (CXRS) diagnostics confirm that both electron temperature and density, and ion temperature

profiles are almost unchanged. These results indicate that inverse Landau damping (growth) caused by the pressure gradient of fast ions, and Landau damping due to bulk electron, bulk ion and fast ion should be almost the same when $N_{||}$ is scanned. When the contribution of the fast ion population as a growth mechanism beats intense continuum damping, shear Alfvén continuum will be forcedly destabilized by fast ion as EPM.

Positive plasma current decreases the rotational transform in the experiment with reversed magnetic field $B_t < 0$. Plasma current is composed of EC-driven current, NB-driven (Ohkawa) current and bootstrap (BS) current in the experiment. Balanced injection of tangential co- and counter-NB can compensate each NB current drive (NBCD) plasma current, and this low bumpiness magnetic configuration minimizes the BS current and maximizes the EC-driven plasma current because the bumpiness can affect the confinement of trapped electrons [26, 30]. Total plasma current of BS and NBCD is estimated less than 0.1 kA at the end of the discharge where the electron density is reached to $0.8\text{x}10^{19}$ m^{-3}. In addition, we did not change NB power and profile of electron temperature and density were not changed in any cases in $N_{||}$ scan experiments, and then, NB-driven current and BS current did not change much in each $N_{||}$ conditions.

The continuum damping is possibly the main damping mechanism of the EPMs as well as GAE. The continuum damping rate is related to local magnetic shear. Figure 3 shows the dependence of the amplitude of magnetic fluctuations on local magnetic shear. In the $N_{||}$ scan, both EPMs and GAE amplitudes are estimated at the same line averaged electron density $\langle n_e \rangle \sim 0.7\text{x}10^{19}$ m^{-3}, the same ECH power $P_{ECH} = 232$ kW and same NBI power $P_{NB} = 400$ kW each. EC-driven plasma current does not saturate at the end of discharge. According to time evolution of rotational transform profile calculated by a current diffusion equation [16], rotational transform at the timing t=0.27 and 0.28 s in which EPM and GAE amplitude was evaluated is almost comparable to the rotational transform in the case of saturated plasma current. The magnetic shear is calculated by a simple cylindrical model with measured plasma current by Rogowski coil and its density profile calculated by TRAVIS code. The effect of three-dimensional structure of the magnetic configuration on the rotational transform modified by plasma current is negligible, especially in EPM and GAE locations.

Amplitude of EPMs and GAEs is plotted as a function of local magnetic shear, which is respectively estimated at normalized minor radius $r/a = 0.8$ and 0.6 where they have a peak around these positions under the $N_{||} = 0.0$ condition according to a beam emission spectroscopy (BES) diagnostic [31]. Since the amplitude of both modes is also a function of electron density, we set the line averaged density $\langle n_e \rangle = 0.7\text{x}10^{19}$ m^{-3} and it is estimated by not instantaneous value of a burst mode but root mean square with the time window of $\delta t = 10$ ms. EPMs and GAE amplitude decrease with an increase of magnetic shear as shown in Figs. 3. EPMs are suppressed but not

fully stabilized by ECCD and other EPMs with $m \sim 4/n = 2$ are destabilized in the condition of $s > 0.07$ although EPMs with $m \sim 2/n = 1$ were successfully stabilized by ECCD in different experimental conditions. In the case of GAE shown in Fig. 3 (b), the mode amplitude gradually decreases with increasing local magnetic shear and finally completely mitigated. The amplitude of density fluctuation of both EPMs and GAE measured by BES show same trend as magnetic fluctuation. Plasma current can change not only magnetic shear but also an MHD equilibrium. We observed frequency of the observed GAE decreases with increasing magnetic shear in $N_{||}$ scan experiment. These effects will be discussed in Sec. 4.

3.2 *Effect of ECH on AEs*

Effects of ECH on fast-ion-driven MHD instabilities has been also studied experimentally in NBI-heated plasmas of Heliotron J. The ECH power is scanned from 114 kW to 282 kW every approximately 60 kW with $N_{||}$ fixed as 0.0 to minimize the ECCD effect on the mode amplitude. Figure 4 shows the time evolution of PSD of the magnetic fluctuation db_θ/dt in the case of (a) the ECH power of $P_{ECH} = 114$ kW and (b) the ECH power of $P_{ECH} = 282$ kW, diamagnetic plasma stored energy, the line averaged electron density, plasma current and the H_α signal. The line averaged density evolves in each ECH power almost in the same method by adjusting gas puffing. The diamagnetic stored energy at higher ECH power is higher than that of lower ECH power because of the increase in electron temperature. The increase in electron temperature measured with a Thomson scattering and electron cyclotron emission measurement (ECE) supports the increase in diamagnetic stored plasma energy. The mode amplitude of the observed modes decreases with increasing ECH power as shown in Figs. 4 (a) and (b). These experimental observations are similar to experimental results on TJ-II, that is, the GAEs and/or HAEs were mitigated with the increasing ECH power by overlapping of ECH injection [13]. The ECH power dependencies on the amplitude of the observed EPMs and GAE are shown in Figs. 5 (a) and (b), respectively. The plasma current ranged from $-0.05 < I_p < 0.05$ kA, that is, almost zero plasma current in order to avoid the ECCD effect on the mode amplitude in these discharges. The amplitude of EPMs is slightly decreased with an increase in ECH power, while the GAE amplitude is clearly suppressed with increasing P_{ECH} as shown in Figs. 5 (a) and (b), respectively.

4. Discussion

We mentioned that the increasing plasma current increases the continuum damping rate via an increase in magnetic shear as discussed in Sec. 3. However, plasma current changes not only magnetic shear but also a

structure of shear Alfvén spectrum due to the change of MHD equilibrium. We investigate the effect of EC-driven plasma current on shear Alfvén spectrum including the comparison of radial structure and frequencies between experimental observed modes and numerical simulations.

Figure 6 shows radial profiles of the observed EPMs and GAE measured with the BES at t = 0.28 s of Fig. 4 (a) where the electron density is $\langle n_e \rangle \sim 0.7 \times 10^{19}$ m^{-3}. The radial profile of the EPMs shown in Fig. 6 (a) is estimated by the electron density fluctuation normalized by averaged electron density at each channel. On the other hand, GAE amplitude is too small to evaluate a mode profile like EPMs. The GAE profile is evaluated by the PSD of electron density fluctuation of the observed modes as shown in Fig. 6 (b). It appears that the observed EPM consists of two modes whose peaks of the amplitude locate at r/a = 0.5 and 0.85. BES data show that the inner mode is firstly destabilized after NBI tuned on (t = 0.20 s) and then the outer mode appears after t = 0.22 s. The change in the phase difference among each magnetic probe supports this timing of the appearance of two modes. Both modes have different toroidal/poloidal mode number according to magnetic probe array data. Since BES data indicate that the mode amplitude of the outer mode is larger than that of the inner mode, mode amplitude and phase difference for the estimation of mode number m/n measured with the magnetic probe array locating outside plasma, as shown in Figs. 2~5, basically reflects the amplitude of the outer mode. The observed GAE is localized around $r/a \sim 0.7$ under the condition of $N_{\|} = 0.0$.

In order to study the effect of EC-driven plasma current on shear Alfvén continua as well as discrete eigenfunctions, we compare these with mode frequencies and profiles of the observed EPMs/GAE where we assume a monotonically peaked profile of plasma current density for the MHD equilibrium reconstruction. This permit the qualitative investigation of the effect of EC-driven plasma current on the MHD equilibrium as well as the shear Alfvén spectrum. Regarding the calculation of shear Alfvén continua in three-dimensional magnetic configuration, the variation of magnetic field strength in toroidal direction induces the toroidal mode coupling of shear Alfvén continua belonging to the same mode family in three-dimensional plasmas [33] including the Heliotron J plasma. For instance, n = 1 continua can couple with continua with n = …-3, -1, 1, 3, 5… in the case of Heliotron J having toroidal field period N_f = 4. This leads that formation of the frequency gap of helicity-induced AE (HAE) in a plasma and high-n Fourier components belonging to the same mode family may affect low-n GAEs. Since the frequencies of HAE gap are usually larger than 1MHz because of a low rotational transform and toroidal mode coupling is weak in the Heliotron J plasmas according to calculation results taken into account of three-dimensional magnetic configuration, we can ignore the effect of toroidal mode coupling in this article.

Figure 7 shows the variation of shear Alfvén continua with m/n = 2/1 and 4/2, and discrete eigenfunctions for the case of n = 1 and 2 where plasma current I_p = 0.0, 0.2 and 0.4 kA in the condition of $B_t < 0$ are considered and the profile of plasma pressure is based on fitted data of electron temperature and density measured with a Thomson scattering system. The calculation of shear Alfvén continua and discrete eigenfunctions is performed by STELLGAP and AE3D codes, respectively. The profiles of rotational transform and estimated current density are also shown in Figs. 7 (c) and (d). The current density profile as shown in Fig. 7 (d) is assumed broader than TRAVIS result and has a peak at the plasma core. The open symbol and horizontal bar around each open symbol in the Figs. 7 (a) and (b) represent a peak position of the discrete eigenfunction and full width at half maximum (FWHM) of each calculated eigenfunction. The closed symbol corresponds to the peak position of the experimentally observed EPMs and GAE measured with BES. The difference of symbol, circle, square and triangle, indicates the amplitude of plasma current. The vertical position of open and closed symbol in Figs. 7 (a) and (b) corresponds to frequency of calculated eigenfunctions and observed EPMs/GAE, respectively. Frequency and peak position of the observed EPMs in the condition of I_p = 0.2 and 0.4 kA are almost similar to that of I_p = 0.0 kA shown as a closed circle in red in Fig. 7 (a).

Frequency and radial peak position of the observed EPMs with m/n = 2/1 (Fig. 6 (a)) agree with the shear Alfvén continuum with m/n = 2/1 around r/a = 0.8 in Fig. 7 (a). EC-driven plasma current does not change the crossing position of the shear Alfvén spectrum with the observed frequency. It is concluded that the suppression of EPMs by ECCD is mainly caused by the increasing continuum damping rate with an increase in local magnetic shear around r/a = 0.8.

In the case of n = 2, we found discrete eigenfunctions laying just below the shear Alfvén continua as shown in Fig. 7 (b). The EC-driven plasma current decreases frequency of the shear Alfvén continuum with m/n = 4/2 and also frequency of discrete eigenfunction. The discrete eigenfunction basically lies around the minimum of shear Alfvén continuum in order to avoid crossing the shear Alfvén continuum. The profiles of discrete eigenfunction in the case of I_p = 0.0 kA is shown in Fig. 8 (a) and (b). The found discrete eigenfunctions are mainly composed of m/n = 4/2 components and has a peak at r/a = 0.6. These results agree with the mode profile and mode number of GAE as shown in Fig. 6 (b). The calculated GAE frequency decreases and moves inwardly with the increasing EC-driven plasma current having the core localized peak profile. Experimental results show that the observed frequency of the GAE is decreased from 145 kHz to 130 kHz and the peak position of GAE seems to be moved slightly inward ($dr/a \sim 0.1$) when plasma current is increased from I_p = 0.0 kA to 0.4 kA under the condition of $\langle n_e \rangle = 0.7 \times 10^{19}$ m^{-3} as shown in Fig. 7 (b). Experimental results cannot be

quantitatively explained by numerical calculations but the tendency of the change of frequency and radial position of the observed GAEs agree with the numerical calculation. The comparison of the calculation of shear Alfvén spectra with experimental results shows that the increasing continuum damping rate with an increase in local magnetic shear by EC-driven current is important for both EPMs and GAEs. Moreover, the increase in plasma current lead to the inward movement of GAEs which would also contribute to the stabilization of GAEs because the continuum damping rate increases more and more toward core.

The difference in the change of frequency and the radial position of GAEs between experimental results and numerical simulation could be caused by the difference of plasma current density profile. The time constant of plasma current L/R (L and R the inductance and resistance) is estimated about 130 ms in the experiment of Heliotron J. It is expected that the BS and NBCD current remain even in the end of discharge where $\langle n_e \rangle = 0.8 \times 10^{19}$ m^{-3}. We showed that only plasma current and the amplitude of both EPMs and GAE are changed when we change $N_{\|}$ in Sec. 3.1. Therefore, EC-driven current mainly affect local magnetic shear rather than the shear Alfvén spectrum. Planned experiments of changing bumpiness will be able to show the effect of BS on a MHD equilibrium.

Regarding the effect of ECH on AEs, the increase in electron temperature leads to the increase in the linear growth rate of modes due to the increase of fast ion beta $\langle \beta_f \rangle$ accompanied with the increase in slowing down time of fast ions. However, experimental results show the opposite trend in the amplitude of both EPMs and GAE. One candidate of the main damping mechanism of both EPMs and GAE in ECH power scan experiments is the collisional damping by a trapped electron, although we do not have any firm experimental evidence to explain that. The collision of trapped electrons with passing ones and ions induce the damping mechanism of TAEs [30]. For typical fusion plasma condition, $v_{Te} >> v_b$ is usually satisfied. Here v_{Te} is the thermal electron velocity, and v_b is the beam ion velocity. Only electrons with $v_{\|} << v_{Te}$ can resonantly interact with fast-ion-driven modes, and trapped electrons satisfies this condition. The damping term due to magnetic curvature drift of passing electrons can be enhanced by existence of the trapped electrons. In helical systems, the collisionless orbit transformation between the locally trapped states and locally passing states changes the collisional damping rate [34]. ECH accelerates electrons in the direction perpendicular to the magnetic field, resulting in enhancement of trapped electron population. Heliotron J has capability to change the trapped electron population by controlling the magnetic configuration, especially the bumpiness component in the Fourier spectra of magnetic field. We have the plan of experiments where poloidal angle of ECH injection and bumpiness will

be scanned to change the ratio of heating power distributed to passing or trapped electron and to change the confinement of trapped electron, respectively.

5. Conclusion

We have performed experiments on suppression of fast-ion-driven MHD instabilities, especially GAE and EPM by applying second harmonic X-mode ECH/ECCD to NBI-heated plasmas in the Heliotron J device. The counter ECCD, which forms a positive magnetic shear, stabilizes both GAEs and EPMs. Some GAEs are fully stabilized when the magnetic shear reaches a critical value. EPMs are suppressed, but not fully stabilized. Since other EPMs newly observed when magnetic shear is increased more, moderate magnetic shear may be required to suppress all the GAEs and EPMs. We showed the experimental results on the positive magnetic shear effect. Co-ECCD experiment is required to clarify the role of sign of the magnetic shear. The comparison of experimental results with calculated shear Alfvén spectrum where we consider the monotonic current density profile indicates that decreasing frequency and inward movement of the observed GAE can be explained by the increase in plasma current although the variation in frequency and radial position of the observed GAE does not agree well with the calculated eigenfunction. The continuum damping mainly contribute to suppress both EPMs and GAEs.

Steady ECH is also found to be effective to suppress both GAEs and EPMs. The mode amplitudes are suppressed with an increase of the ECH power under fixed density condition. In future experiments, we will investigate the effect of magnetic configuration on AEs in Heliotron J, particularly focusing on the trapped electron collisional damping and current density profile. Theoretical work is also an important task to understand the physical mechanism of ECH and ECCD on fast-ion-driven MHD instabilities.

Acknowledgements

The authors are grateful to Dr. N.B. Marushchenko (IPP-Greifswald, Germany) and Dr. D.A. Spong (ORNL, USA) for calculations of the TRAVIS, STELLGAP and AE3D codes are greatly appreciated. The support of the Heliotron J group is also gratefully acknowledged. The work presented was carried out with the support from the auspices of the Collaboration Program of the Laboratory for Complex Energy Processes, Institute of Advanced Energy (IAE), Kyoto University, the National Institute for Fusion Science (NIFS) Collaborative Research Program (NIFS08KAOR010, NFIS10KUHL030), the NIFS/NINS project of Formation of International Network for Scientific Collaboration, the Grant-in-Aid for Scientific Research Ministry of

Education, Culture, Sports, Science and Technology (MEXT) and the Coordinated Working Group Meeting (CWGM).

References (NOTE: NF format)

[1] Wong K.-L. 1999 *Plasma Phys. Control. Fusion* **41** R1

[2] Heidbrink W.W. 2008 *Phys. Plasmas* **15** 055501

[3] Breizman B.N. and Sharapov S.E. 2011 *Plasma Phys. Control. Fusion* **53** 054001

[4] Gorelenkov N.N., Pinches S.D. and Toi K. 2014 *Nucl. Fusion* **54** 125001

[5] Fasoli A. *et al* 2002 *Plasma Phys. Control. Fusion* **44** B159

[6] Testa D., Fasoli A., Solano E., and JET-EFDA Contributors 2003 *Rev. Sci. Instrum.* **74** 1694

[7] Fisch N.J. and Rax J-R. 1992 *Phys. Rev. Lett.* **69** 612

[8] Prater R. 2004 *Phys. Plasmas* **11** 2349

[9] Nagasaki K., *et al* 2005 *Nucl. Fusion* **45** 1608

[10] Van Zeeland M.A. *et al* 2008 *Plasma Phys. Control. Fusion* **50** 035009

[11] Van Zeeland M.A. *et al* 2009 *Nucl. Fusion* **49** 065003

[12] Van Zeeland M.A. *et al* 2016 *Nucl. Fusion* **56** 112007

[13] Nagaoka K. *et al* 2013 *Nucl. Fusion* **53** 072004

[14] Melnikov A.V. *et al* 2016 *Nucl. Fusion* **56** 076001

[15] Melnikov A.V. *et al* 2016 *Nucl. Fusion* **56** 112019

[16] Nagasaki K. *et al* 2013 *Nucl. Fusion* **53** 113041

[17] Yamamoto S. *et al* 2014 *25th IAEA Fusion Energy Conference (St Petersburg, Russia, 13-18 Oct. 2014)*

[18] Rosenbluth M.N., Berk H.L., Van Dam J.W., Lindberg D.M. 1992 *Phys. Rev. Lett.* **68** 596

[19] Berk H.L., Van Dam J.W., Guo Z., and Lindberg D. M. 1992 *Phys. Fluids* B **4** 1806

[20] Wakatani M. *et al* 2000 *Nucl. Fusion* **40** 569

[21] Obiki T. *et al* 2000 *Plasma Phys. Control. Fusion* **42** 1151

[22] Yamamoto S. *et al* 2007 *Fusion Sci. Technol*. **51** 92

[23] Weller A. *et al* 2001 *Phys. Plasmas* **8** 931

[24] Nagasaki K. *et al* 2010 *Contrib. Plasma Phys*. **50** 656

[25] Maruchchenko N.B. *et al* 2007 *Plasma Fusion Res.* **2** S1129

[26] Nagasaki K. *et al* 2011 *Nucl. Fusion* **51** 103035

[27] Hirshman S.P. and Whitson J.C. 1983 *Phys. Fluids* **26** 3553

[28] Spong D.A., Sanchez R. and Weller A. 2003 *Phys. Plasmas* **10** 3217

[29] Spong D.A., D'Azevedo E. and Todo Y. 2010 *Phys. Plasmas* **17** 022106

[30] Motojima G., *et al* 2007 *Nucl. Fusion* **47** 1045

[31] Kobayashi S. *et al* 2012 *Rev. Sci. Instrum*. **83** 10D535

[32] Gorelenkov N.N. and Sharapov S.E. 1992 *Physca Scripta* **45** 163

[33] C. Schwab, 1993 *Phys. Fluids B* **5** 3195

[34] Kolesnichenko Ya.I. and Marchenko V.S. 2004 *Phys. Plasmas* **11** 4616

Figure caption

Figure 1: Calculated profiles of (a) EC-driven plasma current density j_{EC} by TRAVIS code and (b) the rotational transform which is simply estimated in cylindrical geometry by adding the poloidal magnetic field produced by calculated j_{EC} profile to the vacuum magnetic field. Solid line in blue, dotted line in red and broken line in black in Figs. (a) and (b) indicates parallel refractive index $N_{||}$=0.0, 0.1 and 0.2, respectively. (c) Calculated deposition profile of ECH by TRAVIS code with P_{ECH}=240 kW and $N_{||}$ = 0.00.

Figure 2: Time evolution of (a) power spectrum density (PSD) of magnetic fluctuations in the case of non-ECCD corresponding to $N_{||}$ = 0.00, (b) also PSD in the case of ECCD ($N_{||}$ = 0.15), (c) plasma stored energy measured by diamagnetic loop and superposed injection timing of ECH and two NBIs (d) the line averaged electron density measured by a FIR interferometer, (e) plasma current and (f) the Lyman alpha line of both $N_{||}$=0.00 and 0.15. The solid line in blue and broken line in red respectively represent the case of $N_{||}$ = 0.00 and 0.15 in Figs. (c) - (f).

Figure 3: Magnetic shear dependence of normalized magnetic fluctuation b_θ/B_t of the observed (a) EPMs with m~2/n=1 and (b) GAE with m~4/n=2 at the line averaged density $\langle n_e \rangle \sim 0.7\text{x}10^{19}$ m^{-3}. Differences of symbol and color indicate the difference of $N_{||}$. Estimated magnetic shear is evaluated at the measured peak position of EPMs and GAE under condition of $N_{||}$ = 0.00.

Figure 4: Time evolution of (a) PSD of magnetic fluctuations in the case of the ECH power of P_{ECH}=119 kW, (b) also PSD in the case of the ECH power of P_{ECH}=282 kW, (c) plasma stored energy measured by diamagnetic loop and superposed injection timing of ECH and two NBIs (d) the line averaged electron

density measured by a FIR interferometer, (e) plasma current and (f) the Lyman alpha line of both P_{ECH}=119 and 282 kW. The solid line in blue and broken line in red respectively represent P_{ECH}=119 and 282 kW in Figs. (c) - (f).

Figure 5: ECH power dependence of normalized magnetic fluctuation b_θ/B_t of the observed (a) EPMs with m~2/n=1 and (b) GAE with m~4/n=2 at the line averaged density $\langle n_e \rangle \sim 0.7\text{x}10^{19}$ m^{-3}.

Figure 6: Radial profiles of the observed (a) EPMs with $m \sim 2/n = 1$ as density fluctuation normalized by local averaged electron density and GAE $m \sim 4/n = 2$ as PSD of density fluctuation measured with BES measurement under the condition of $\langle n_e \rangle = 0.7\text{x}10^{19}$ m^{-3} and $N_{||} = 0.0$. The noise level is also plotted with a square open symbol and dotted line in (a) and (b).

Figure 7: Shear Alfvén continua (a) with m/n=2/1 and (b) 4/2 accompanying with discrete eigenfunctions. Open symbol and horizontal bar around open symbol indicate the peak position of eigenfunctions and FWHM of them. Closed symbol indicates the experimental result measured by BES. The difference of symbol means the amplitude of plasma current I_p=0.0, 0.2 and 0.4 kA. (c) profiles of rotational transform with finite beta effect plasma current and without plasma. (d) current density profile.

Figure 8: Profiles of n=2 GAE with m=4 and m=3 corresponding to eigenfunctions (electrostatic potential) in Fig. 7 (b) under the condition of $I_p = 0.0$ kA.

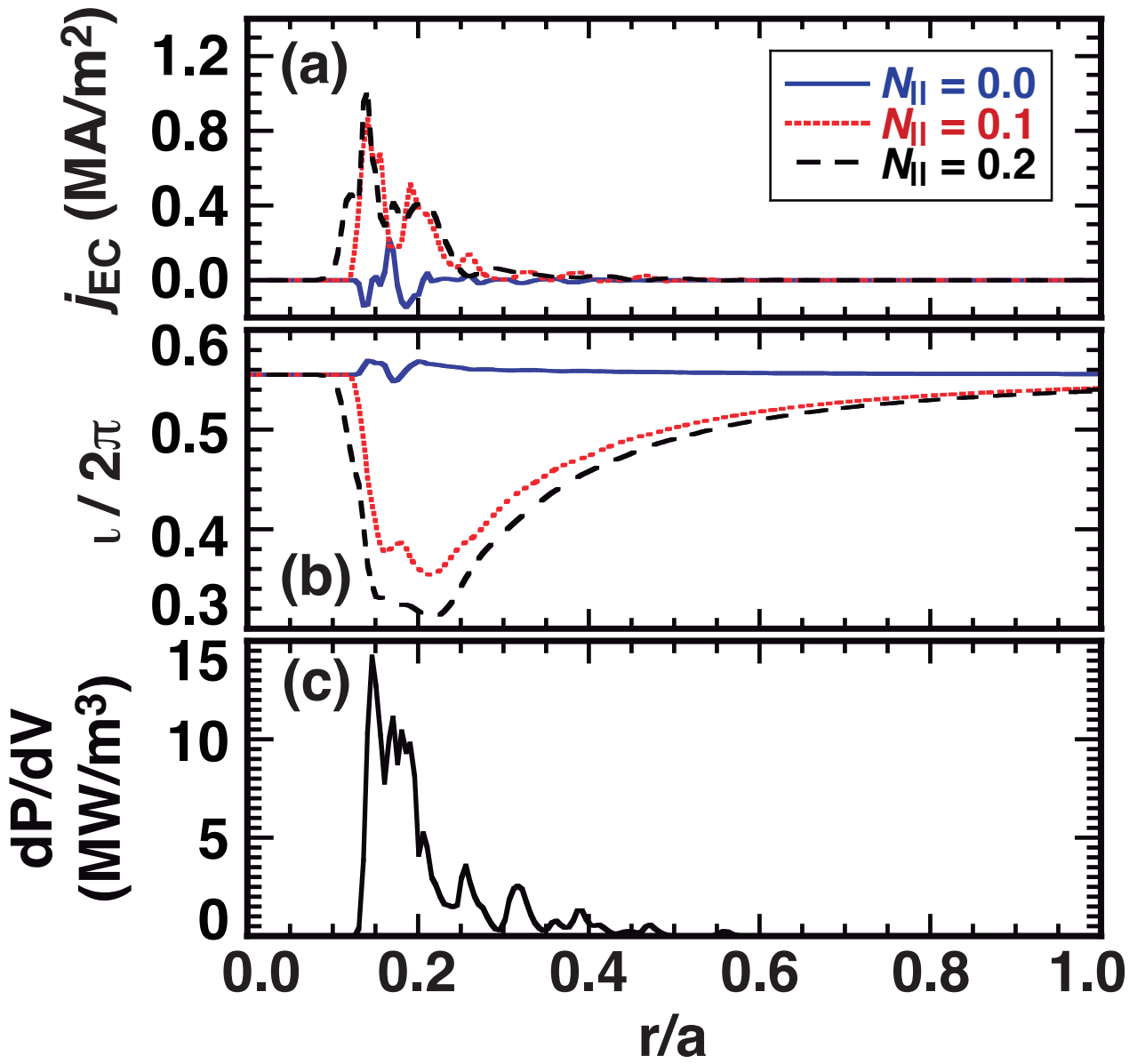

Fig. 1, S. Yamamoto *et al*

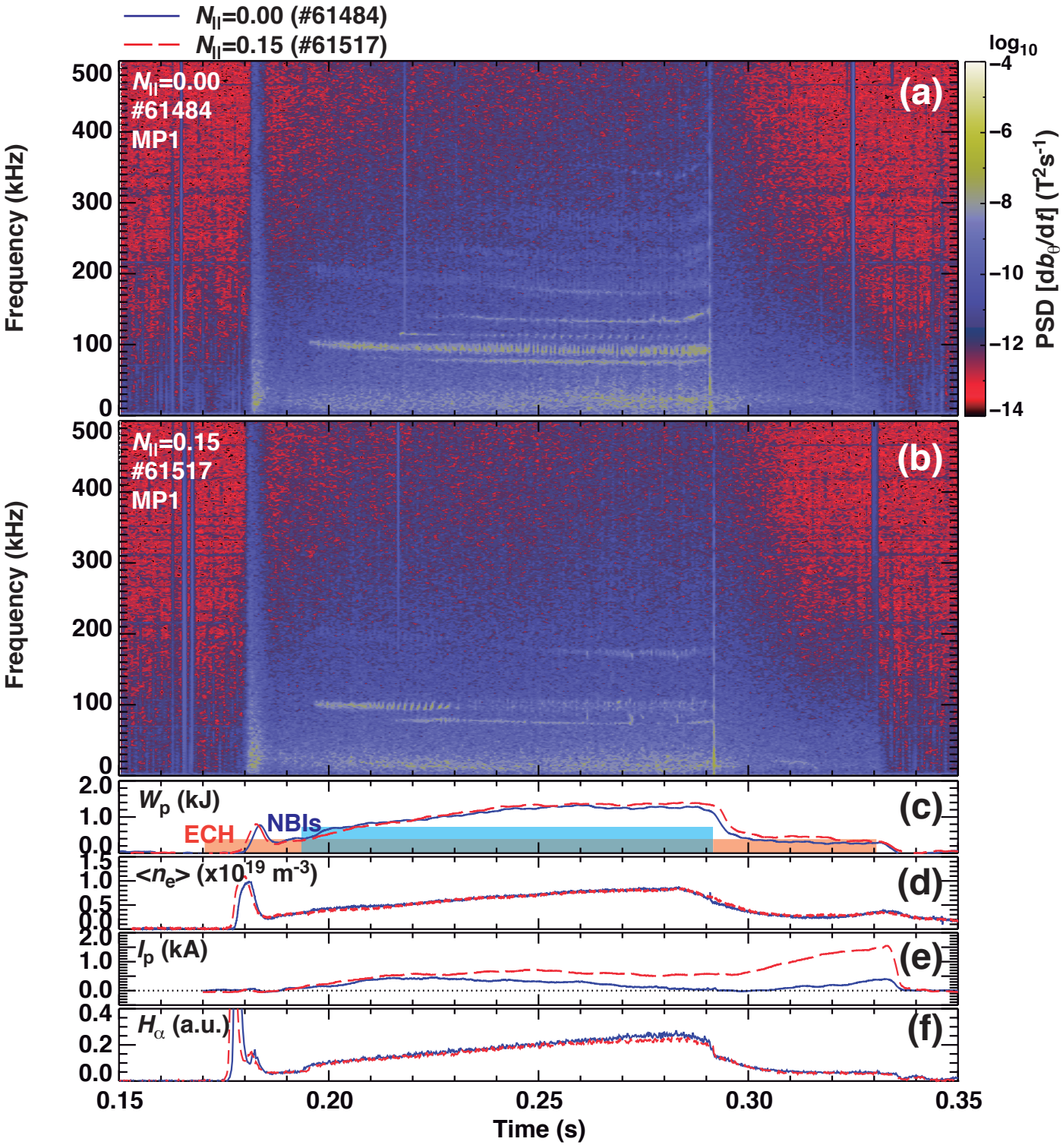

Fig. 2, S. Yamamoto *et al*

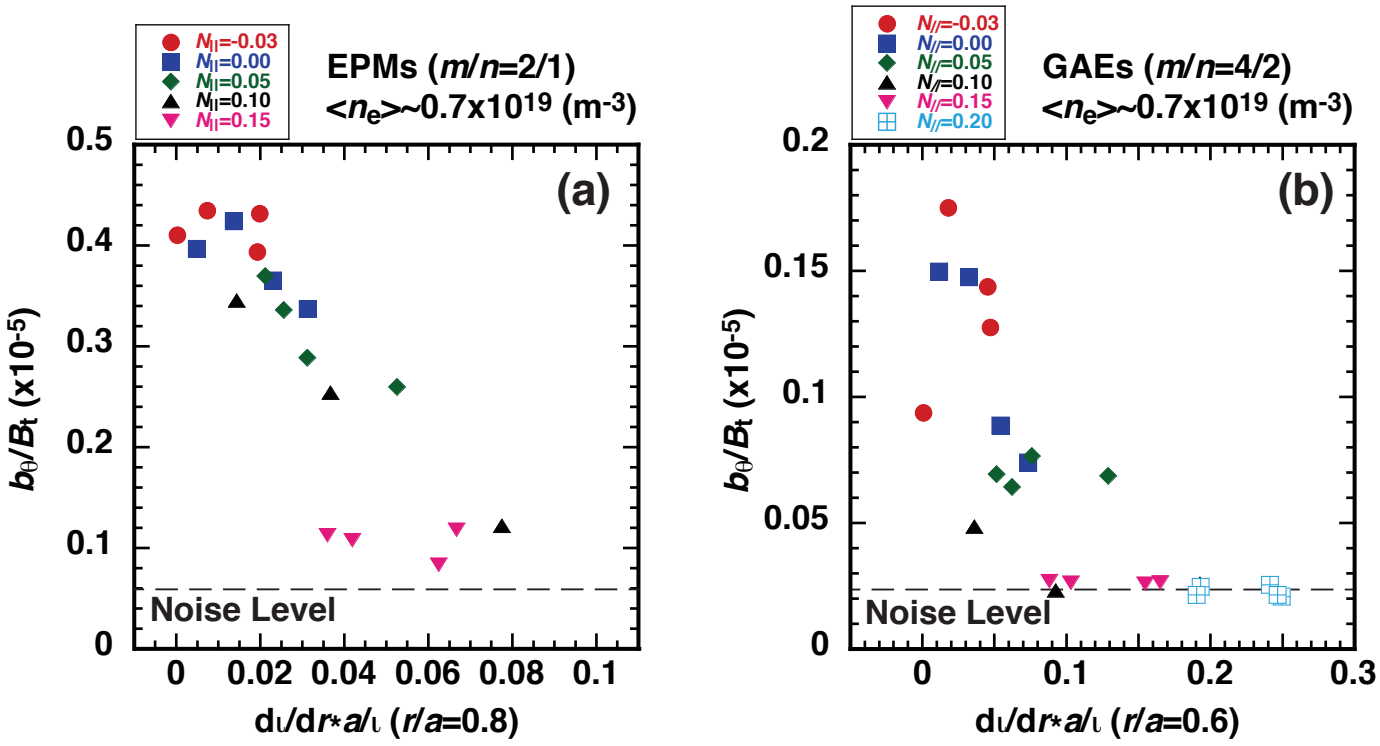

Fig. 3, S. Yamamoto *et al*

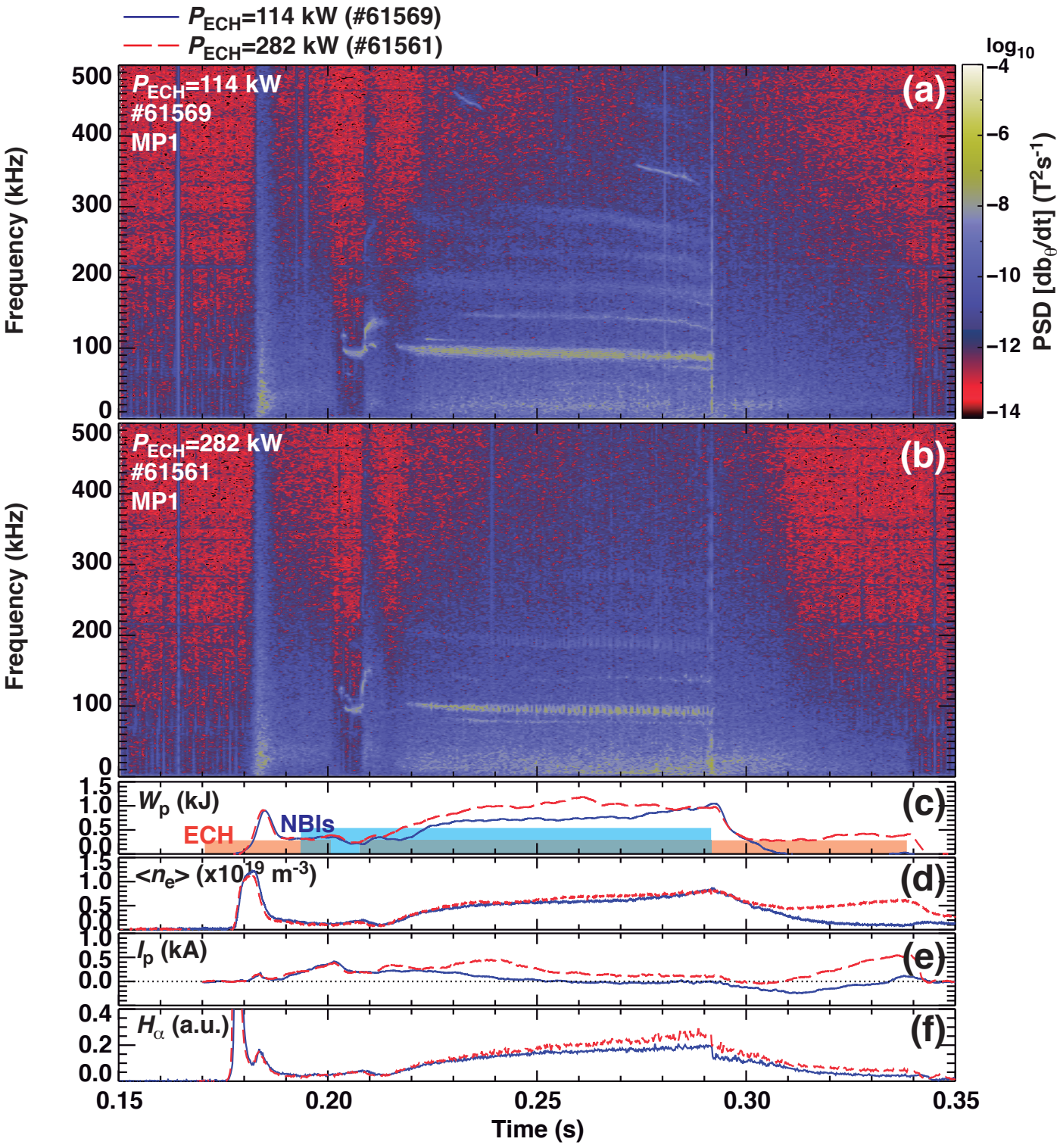

Fig. 4, S. Yamamoto *et al*

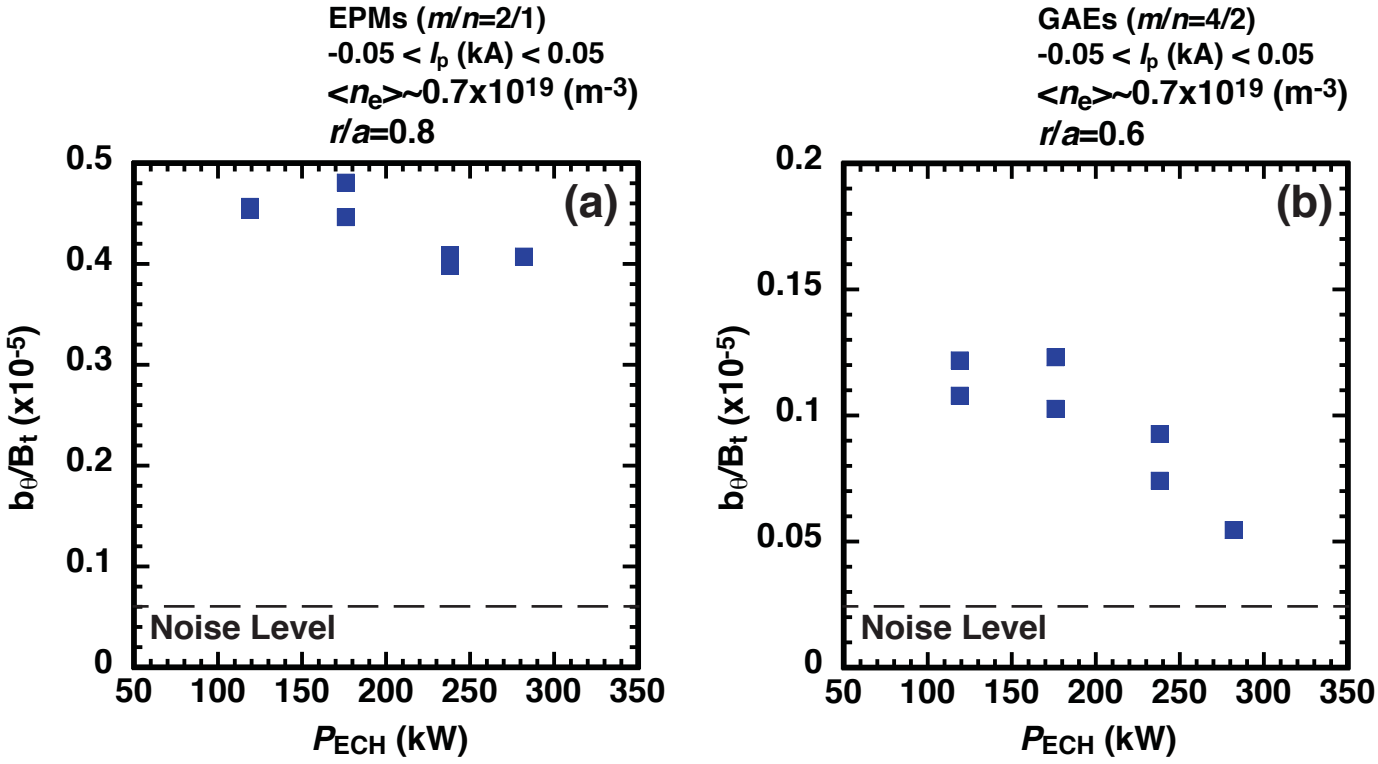

Fig. 5, S. Yamamoto *et al*

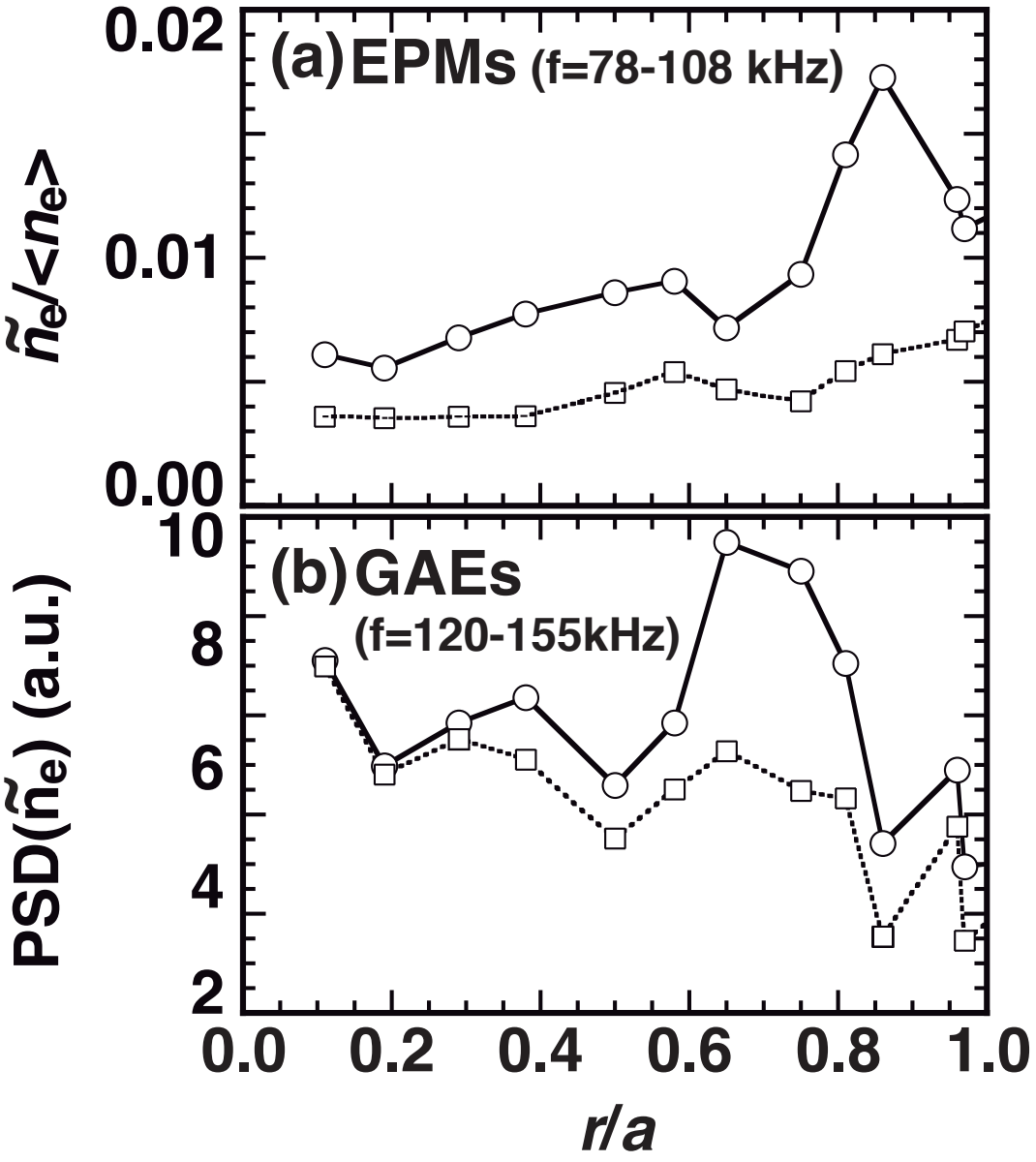

Fig. 6, S. Yamamoto et al.

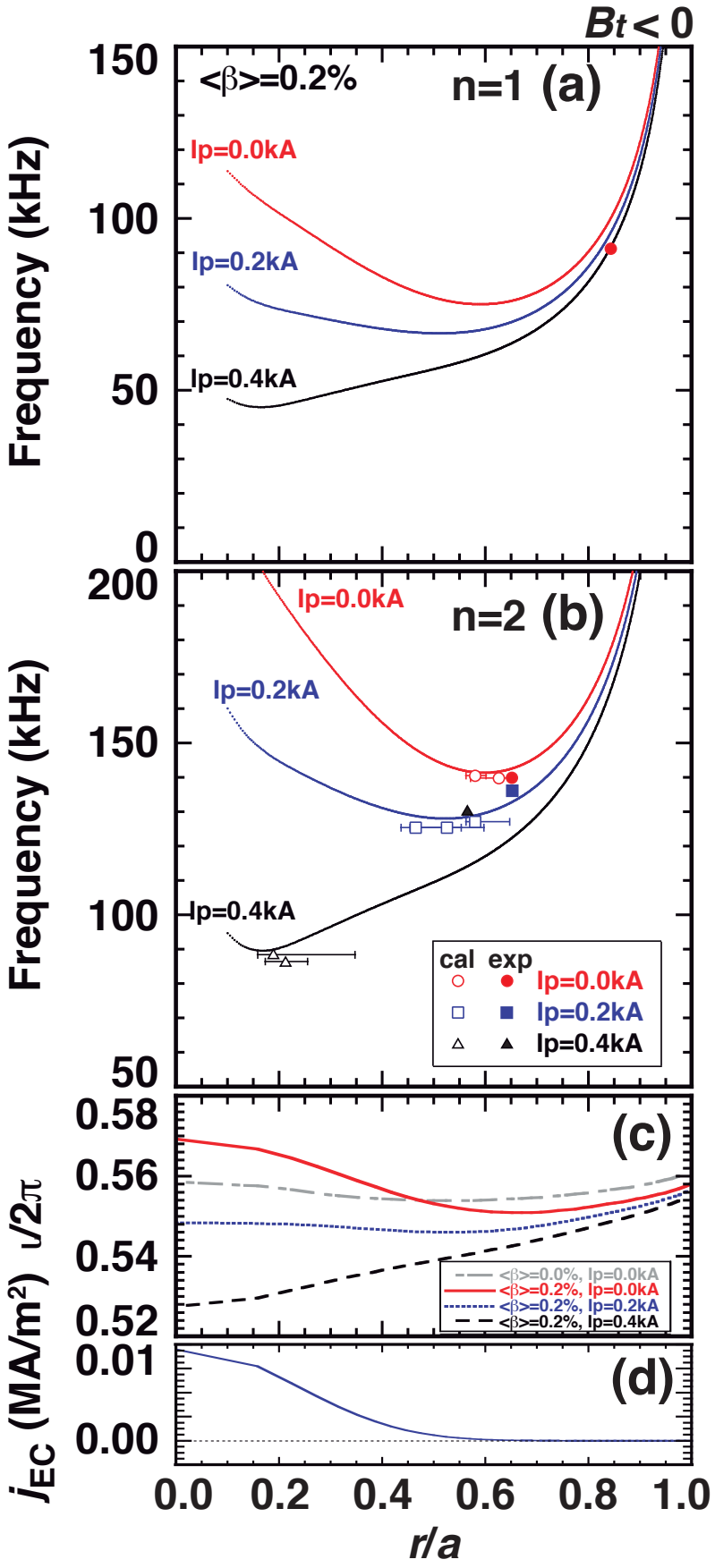

Fig. 7, S. Yamamoto *et al*

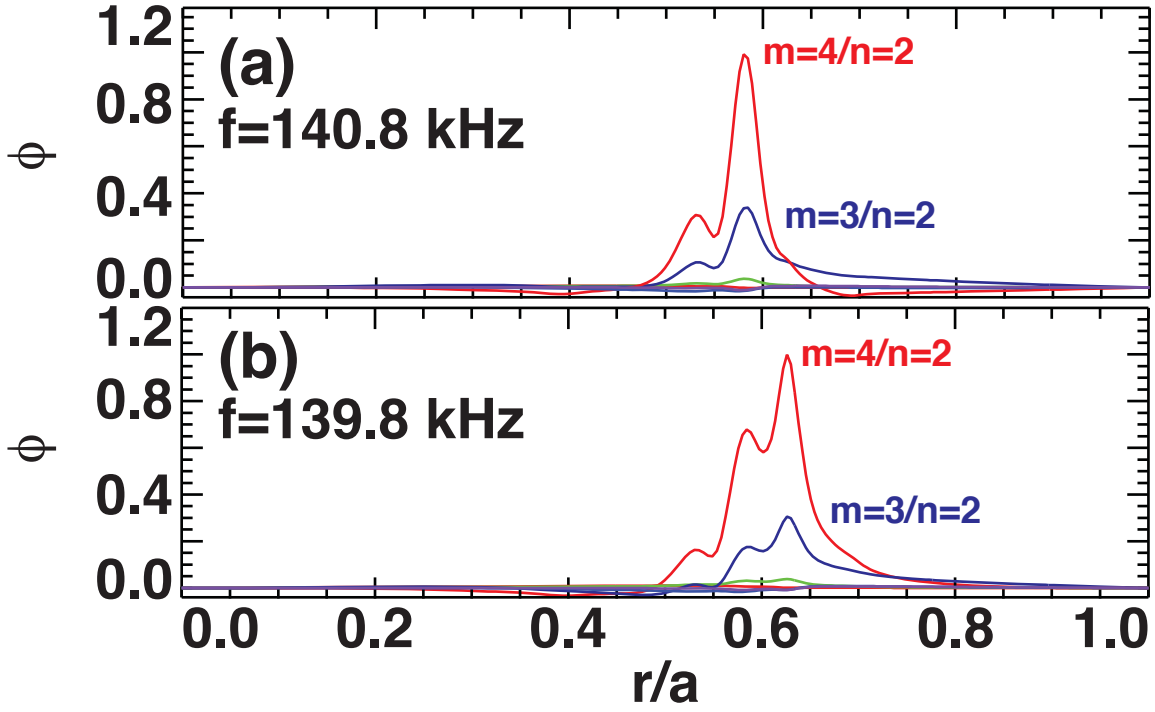

Fig. 8, S. Yamamoto *et al*